

Boosting Semi-Supervised 2D Human Pose Estimation by Revisiting Data Augmentation and Consistency Training

Huayi Zhou¹ Mukun Luo¹ Fei Jiang² Yue Ding¹ Hongtao Lu¹

¹Shanghai Jiao Tong University ²Chongqing Academy of Science and Technology

{sjtu_zhy, luomukun}@sjtu.edu.cn, fjiang@mail.ecnu.edu.cn, {dingyue, htlu}@sjtu.edu.cn

Abstract

The 2D human pose estimation is a basic visual problem. However, supervised learning of a model requires massive labeled images, which is expensive and labor-intensive. In this paper, we aim at boosting the accuracy of a pose estimator by excavating extra unlabeled images in a semi-supervised learning (SSL) way. Most previous consistency-based SSL methods strive to constraint the model to predict consistent results for differently augmented images. Following this consensus, we revisit two core aspects including advanced data augmentation methods and concise consistency training frameworks. Specifically, we heuristically dig various collaborative combinations of existing data augmentations, and discover novel superior data augmentation schemes to more effectively add noise on unlabeled samples. They can compose easy-hard augmentation pairs with larger transformation difficulty gaps, which play a crucial role in consistency-based SSL. Moreover, we propose to strongly augment unlabeled images repeatedly with diverse augmentations, generate multi-path predictions sequentially, and optimize corresponding unsupervised consistency losses using one single network. This simple and compact design is on a par with previous methods consisting of dual or triple networks. Furthermore, it can also be integrated with multiple networks to produce better performance. Comparing to state-of-the-art SSL approaches, our method brings substantial improvements on public datasets. Code is released for academic use¹.

1. Introduction

2D human pose estimation (HPE) aims to detect RGB images and represent human parts as sparse keypoint locations. These keypoints contain concise information about people's shapes and poses, which are the basis of many visual tasks such as action recognition [12, 44], person re-identification [32, 53] and 3D human shape regression

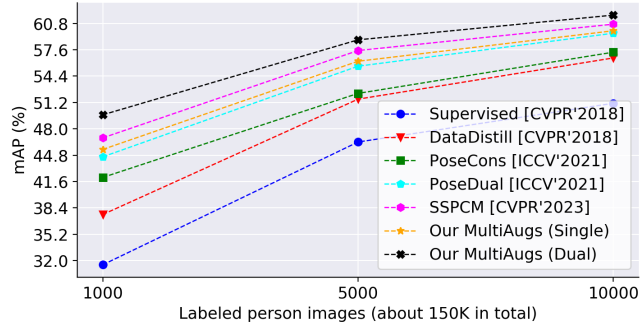


Figure 1. Comparison between state-of-the-art SSHPE methods and our proposed MultiAugs on the COCO dataset.

[28, 29]. Modern data-driven HPE task has been substantially improved by generous deep supervised learning approaches [4, 8, 35, 39, 43, 45]. This greatly benefits from the collection and annotation of numerous large-scale public HPE datasets [1, 24, 38]. However, compared to image classification and detection tasks needing plain labels, obtaining accurate 2D keypoints of massive images is laborious and time-consuming. To this end, some researches [17, 25, 37, 42] try to alleviate this problem by introducing the semi-supervised 2D human pose estimation (SSHPE), which can subtly leverage extensive easier obtainable yet unlabeled 2D human images in addition to partial labeled data to obtain performance improving.

Although SSHPE methods [17, 42] have largely improved the accuracy of SSHPE task, they overlooked two fundamental questions:

1) **How to judge the discrepancy of unsupervised data augmentations with different difficulty levels?** In [42], as shown in Fig. 2 (a), for a batch of unlabeled images \mathbf{I} , its easy augmentation \mathbf{I}_e and hard augmentation \mathbf{I}_h are generated separately. Then, predicted heatmap \mathbf{H}_e of \mathbf{I}_e is used to teach the network to learn the harder counterpart \mathbf{I}_h by applying unsupervised loss with its yielded heatmap \mathbf{H}_h . [42] finds that the large gap between two augmentations ($\mathbf{I}_e, \mathbf{I}_h$) matters. Essentially, this is a pursuit for more advanced data augmentations in SSHPE. To rank augmentations of different difficulty levels, [42] observed precision degrada-

¹<https://github.com/hnuzhy/MultiAugs>

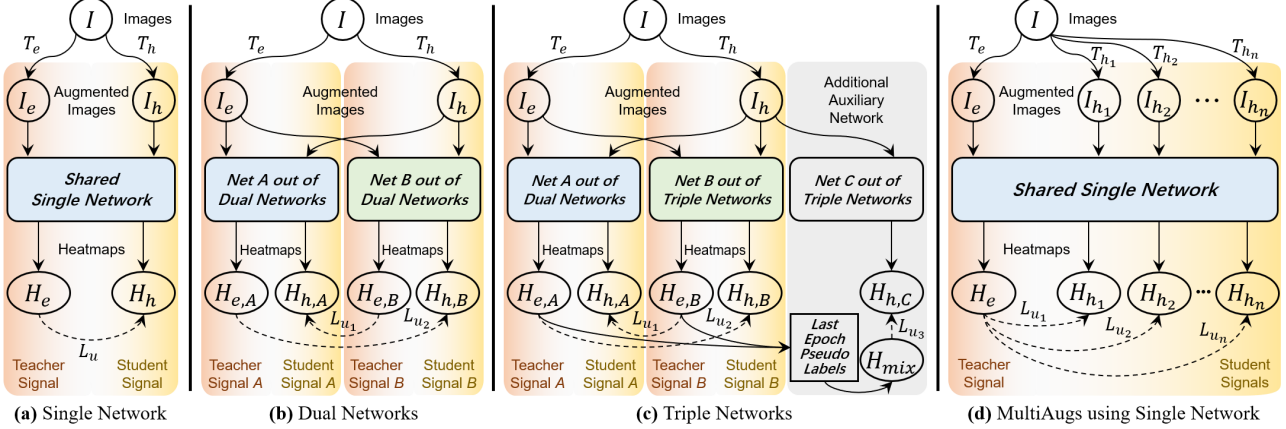


Figure 2. Frameworks of existing SSHPE methods including (a) Single-Network and (b) Dual-Network proposed by [42], and (c) Triple-Network proposed by [17]. We propose a novel framework (d) MultiAugs based on the Single-Network, which can utilize multiple hard augmentations and facilitate multi-path unsupervised consistency training.

tion of a pretrained model by testing it on a dataset after corresponding augmentation. We declare that this manner is not rigorous, but requires independent training for each data augmentation. Furthermore, we discovered the synergistic effects of existing data augmentations [10, 11, 13, 48, 51]. That is, through reasonable sequential augmentations, more superior novel augmentation combinations can be conveniently generated. They have favorable interpretability and omit painstaking manual designs.

2) How to generate multiple unsupervised signals for consistency training efficiently and concisely? Previous work [42] proposes the baseline consistency training framework learning on the easy-hard pair ($\mathbf{I}_e, \mathbf{I}_h$) unsupervisedly using a Single-Network. It also built a more complicated Dual-Network as in Fig. 2 (b) with parameters doubled for cross-training of two easy-hard pairs. SSPCM [17] even constructs a Triple-Network as in Fig. 2 (c) for interactive training of three easy-hard pairs. This pattern of adding the number of networks with the increase of unsupervised signal pairs can certainly bring gains, but it is cumbersome and will decelerate the training speed proportionally. In practice, considering that augmentations are always performed on the same input, we can repeatedly augment \mathbf{I} multiple times with n diverse hard augmentations, and generate multi-path easy-hard pairs $\{(\mathbf{I}_e, \mathbf{I}_{h_1}), (\mathbf{I}_e, \mathbf{I}_{h_2}), \dots, (\mathbf{I}_e, \mathbf{I}_{h_n})\}$. In this way, as shown in Fig. 2 (d), we can use only one network to optimize n pairs of unsupervised losses simultaneously. This is also applicable to multiple networks. We validated the effectiveness of this compact design in experiments. Combined with various advanced augmentations, the performance of our method with one Single-Network can exceed the original Dual-Network [42], and be close to that of SSPCM based on a Triple-Network.

In this paper, we mainly revisit above two questions to boost SSHPE. In summary, our contributions are as follows:

- We comprehensively evaluated the difficulty level of existing unsupervised data augmentation methods suitable for the SSHPE task, discovered and validated the synergistic effect of different augmentations by properly combining them in sequence, and presented novel keypoint-related augmentation paradigms.
- We proposed to generate multi-path predictions of separately augmented hard samples through only one single model, instead of adding auxiliary networks during training. Thus, we can optimize multiple unsupervised losses efficiently and concisely. This succinct design can conveniently integrate various superior augmentations.
- We achieved new state-of-the-art results on many public SSHPE benchmarks with less training time and parameters under same settings of previous methods.

2. Related Work

2D Human Pose Estimation (HPE). Current methods can be divided into two groups: top-down and bottom-up. The top-down methods [35, 39, 43] firstly detect all persons in one image, and then conduct keypoints localization of each cropped person using expanded human bounding boxes. With reliable boxes, they can be combined with heatmap prediction to obtain state-of-the-art pose estimation results. The bottom-up methods [4, 8, 45] directly detect all keypoints, and then group them into individual skeletons by applying post-processing strategies. They usually consume almost constant time with increasing people in the input image. However, all these HPE methods are based on supervised learning needing laboriously labeled keypoints. We try to alleviate this problem by using semi-supervised learning techniques for boosting performance.

Semi-Supervised Learning (SSL). SSL is invented for the classification task to improve performance by exploiting a small set of labeled data and a large set of unlabeled

data. They can be categorized into pseudo-label (PL) based [27, 31, 33, 41] and consistency-based [2, 21, 36, 40, 49]. PL-based methods iteratively add unlabeled images into the training data by pseudo-labeling them with a pretrained or gradually enhanced model. It needs to find suitable thresholds to mask out uncertain examples with low-confidence, which a crucial yet tricky issue. Consistency-based methods enforce the model output to be consistent when it is randomly perturbed. They have shown to work well on many benchmarks for an intuitive and universal sense that a good model should be robust to any tractable input change. For example, MixMatch [2] combines the consistency regularization with the entropy minimization to obtain confident predictions. FixMatch [33] utilizes a weak-to-strong consistency regularization and integrates the pseudo labeling to leverage unlabeled data. FlexMatch [49] introduces the curriculum learning based on FixMatch. These SSL methods give us primitive inspirations to propose our solutions.

Semi-Supervised Human Pose Estimation (SSHPE). The SSHPE task is relatively less-studied comparing to other visual tasks such as classification and object detection. A few representative methods are based on either pseudo labeling [34, 37] or consistency training [17, 25, 42]. SSKL [25] designs a semantic keypoint consistency constraint to learn invariant representations of same keypoints. It has been evaluated on small-scale HPE benchmarks MPII [1] and LSP [18], instead of the larger COCO [24]. Following it, PLACL [37] introduces the curriculum learning by automatically selecting dynamic thresholds for producing pseudo-labels via reinforcement learning. Inspired by co-training [30] and dual-student [20], Dual-Network [42] points out the typical collapsing problem in SSHPE, and proposes the easy-hard augmentation pair on the same input to imitate teacher-student signals without relying on Mean Teacher [36]. SSPCM [17] extends the Dual-Network into Triple by adding an auxiliary teacher for interactive training in multi-steps. It designs a handcrafted pseudo-label correction module based on the predicted position inconsistency of two teachers, and has achieved state-of-the-art performances. We revisit the less efficient consistency training patterns in [17, 42], and propose to upgrade the Single-Network furtherly by multi-path predictions.

Unsupervised Data Augmentations. The UDA [40] has emphasized and verified the key role of high-quality noise injection (*e.g.*, data augmentations) in improving unsupervised consistency training. It utilizes advanced augmentations [9, 10] to largely promote the performance on SSL classification. Then, [42] transfers the positive correlation between strong data augmentation operations and SSL performance to the HPE field. It also introduces a more advanced augmentation called Joint Cutout inspired by random Cutout [11]. Following these settings, SSPCM [17] provides a harder augmentation Cut-Occlude that is similar

to CutMix [48] but sensitive to human keypoints. In this paper, we thoroughly revisit existing data augmentations suitable for SSHPE, give a rank of their difficulty levels by strictly controlled trainings, and produce simple paradigms for getting novel superior joint-related augmentations.

3. Proposed Method

Our method is based on [42], which will be briefly reviewed in Sec. 3.1. Then, we answer two questions raised in Sec. 1 about data augmentation methods and consistency training frameworks in Sec. 3.2 and Sec. 3.3, respectively. Finally, we summarize our overall framework of hybrid multiple augmentations (MultiAugs) in Sec. 3.4.

3.1. Preliminaries

The task of 2D HPE is to detect k body joints in an image $\mathbf{I} \in \mathbb{R}^{h \times w \times 3}$. The state-of-the-art methods tend to estimate k Gaussian heatmaps $\mathbf{H} \in \mathbb{R}^{\frac{h}{s} \times \frac{w}{s} \times k}$ downsampled s times. For inference, each keypoint is located by finding the pixel with largest value in its predicted heatmap. We denote the labeled and unlabeled training sets as $\mathcal{D}^l = \{(\mathbf{I}_i^l, \mathbf{H}_i^l)\}_{i=1}^N$ and $\mathcal{D}^u = \{\mathbf{I}_i^u\}_{i=1}^M$, respectively. The \mathbf{H}^l are ground-truth heatmaps generated using 2D keypoints. For supervised training of the network f , we calculate the MSE loss:

$$\mathcal{L}_s = \mathbb{E}_{\mathbf{I} \in \mathcal{D}^l} \|f(T_e(\mathbf{I})) - T_e(\mathbf{H})\|^2 \quad (1)$$

where T_e represents an easy affine augmentation including a random rotation angle from $[-30^\circ, 30^\circ]$ and scale factor from $[0.75, 1.25]$ (denoted as T_{A30}). For unlabeled images, we calculate the unsupervised consistency loss:

$$\mathcal{L}_u = \mathbb{E}_{\mathbf{I} \in \mathcal{D}^u} \|T_{e \rightarrow h}(f(T_e(\mathbf{I}))) - f(T_h(\mathbf{I}))\|^2 \quad (2)$$

where T_h is a harder augmentation with strong perturbations than affine-based T_e . The $T_{e \rightarrow h}$ means a known affine transformation on heatmaps if T_h contains additional rotation and scaling operations. Through this way, we can obtain a paired easy-hard augmentations $(\mathbf{I}_e, \mathbf{I}_h) = (T_e(\mathbf{I}), T_h(\mathbf{I}))$ for generating corresponding teacher signals and student signals. As suggested in [42], to avoid collapsing, we should call the detach operator on teacher signals to stop gradients propagation during training.

3.2. Synergy between Augmentations

The core of the easy-hard pair paradigm $(\mathbf{I}_e, \mathbf{I}_h)$ is a more advanced augmentation. For this reason, Dual-Network [42] and SSPCM [17] propose pseudo keypoint-based augmentations Joint Cutout (T_{JC}) and Joint Cut-Occlude (T_{JO}), respectively. They also reach a similar yet crude conclusion about difficulty levels of existing augmentations: $\{T_{JO}, T_{JC}\} > \{T_{RA}, T_{CM}, T_{CO}, T_{MU}, T_{A60}\}$, where T_{RA} , T_{CM} , T_{CO} and T_{MU} are RandAugment [10],

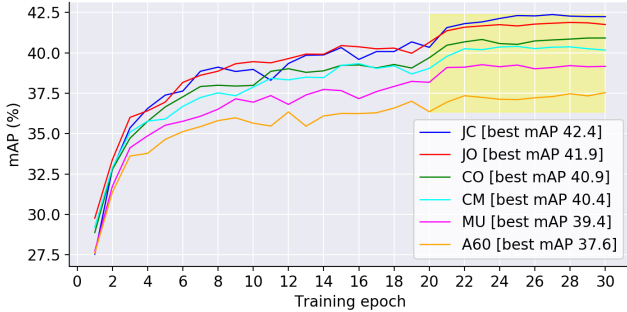


Figure 3. Comparison of applying different easy-hard pairs for training a Single-Network model as described in Fig. 2 (a). We can sort these six augmentations indisputably based on either best mAP results or distinct convergence curves.

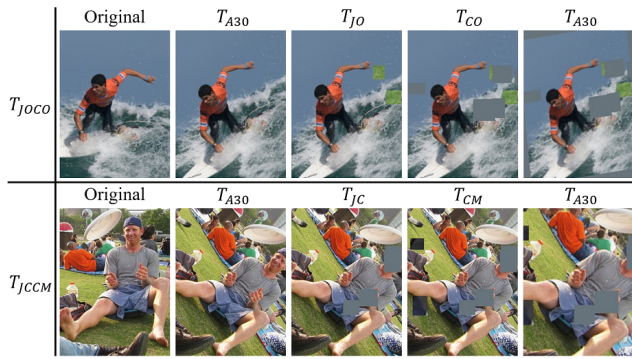


Figure 4. Illustrations of two novel superior combinations T_{JOCO} and T_{JCCM} . Either of them is a sequential operations using ready-made collaborative augmentation. And T_{JO} and T_{CM} introduce extra patches cropped from other images which are not displayed.

CutMix [48], Cutout [11] and Mixup [51], respectively. The T_{A60} is a sum of two T_{A30} . We give them a new ranking by conducting more rigorous trainings one-by-one. The T_{RA} is removed for it contains repetitions with T_{CO} and T_{A60} . As shown in Fig. 3, we divide the rest by their distinguishable gaps into four levels: $\{T_{JC}, T_{JO}\} > \{T_{CO}, T_{CM}\} > \{T_{MU}\} > \{T_{A60}\}$. Instead of laboriously proposing stronger augmentations, we consider *whether we can perform two or more augmentations in sequence to obtain a superior combination as an alternative*.

In fact, after performing joint-related augmentations JO or JC on one image, we can continue to perform some joint-unrelated augmentations such as T_{CM} , T_{CO} and T_{MU} on random areas. As shown in Fig. 4, applying T_{JOCO} (a T_{CO} after T_{JO}) or T_{JCCM} (a T_{CM} after T_{JC}) will bring harder samples for generating more effective student signals, but not destroy the semantic information on the image visually. We call this discovery the **synergistic effect** between different augmentations. The T_{A60} can serve as an essential factor in any T_h for keeping the geometric diversity. If selecting from the rest five basic augmentations, there are up to 26 combinations ($2^5 - \binom{5}{0} - \binom{5}{1}$). It seems that optimal combinations are time-consuming to acquire.

Fortunately, not arbitrary number or kind of augmentations are collaborative. For example, adding a global T_{MU} does not make sense for the HPE task. Stacking augmentations with the similar perturbation type (e.g., $T_{JO} \sim T_{CM}$ and $T_{JC} \sim T_{CO}$) or difficulty level (e.g., $T_{JO} \sim T_{JC}$ and $T_{CM} \sim T_{CO}$) may not bring significant gain. And accumulating too many augmentations (e.g., three or four) will be profitless or even harmful for seriously polluting the raw image. Following these simplistic assumptions, we nominate the most likely two novel superior combinations: T_{JOCO} and T_{JCCM} . A typical case of setting T_e as T_{A30} and T_h as T_{JOCO} for getting corresponding easy teacher signals \mathbf{H}_e and hard student signals \mathbf{H}_h is shown as below:

$$\begin{aligned} \mathbf{H}_e &= T_{A30 \rightarrow A60}(f(\mathbf{I}_e)), \quad \mathbf{I}_e = T_{A30}(\mathbf{I}) \\ \mathbf{H}_h &= f(\mathbf{I}_h), \quad \mathbf{I}_h = T_{A30}(T_{CO}(T_{JO}(T_{A30}(\mathbf{I})))) \end{aligned} \quad (3)$$

where T_{A60} is default to T_h , and decomposed into two separate T_{A30} for being compatible with T_e . More relevant selection discussion, comparative analysis and performance verification are presented in ablation studies.

3.3. Multi-path Consistency Losses

To further amplify the advantage of easy-hard augmentation, [42] adopts two independent networks containing two easy-hard pairs for producing two consistency losses. SSPCM [17] continues this route by designing a Triple-Network with three easy-hard pairs. Meanwhile, some SSL methods construct multi-view inputs for unlabeled data without adding accompanying networks. For example, SwAV [5] enforces the local-to-global consistency among a bag of views with different resolutions. ReMixMatch [3] feeds multiple strongly augmented versions of an input into the model for training. Therefore, we wonder whether such a simple idea can also benefit the SSHPE task.

Specifically, rather than feeding a single hard augmentation \mathbf{I}_h into the model, we independently yield n strongly augmented inputs $\mathcal{I}^n = \{\mathbf{I}_{h_1}, \mathbf{I}_{h_2}, \dots, \mathbf{I}_{h_n}\}$ from \mathbf{I} by applying n hard data augmentations $\mathcal{T}^n = \{T_{h_1}, T_{h_2}, \dots, T_{h_n}\}$ accordingly. The augmentation set \mathcal{T}^n is de-emphasized in order and non-deterministic, and will generate distinct multi-path augmented inputs \mathcal{I}^n . Then, we can calculate n -stream heatmaps $\mathcal{H}^n = \{f(T_{h_i}(\mathbf{I}_{h_i}))\}_{i=1}^n\}$. This multi-path augmentation framework is illustrated in Fig. 2 (d). For regularizing n easy-hard pairs, we obtain multi-path consistency losses using Eq. 2 in separate, and optimize them jointly by applying multi-loss learning:

$$\mathcal{L}_u^* = \mathbb{E}_{\mathbf{H}_{h_i} \in \mathcal{H}^n} \sum_{i=1}^n \|\mathbf{H}_e - \mathbf{H}_{h_i}\|^2 \quad (4)$$

where \mathbf{H}_e and \mathbf{H}_{h_i} are generated as dissected in Eq. 3. The \mathbf{H}_e keeps constant for each \mathbf{H}_{h_i} . Comparably, Data Distill [31] applies a single model to multiple transformations

of unlabeled data to train a student model. Then, it ensembles these predictions to obtain keypoint locations, and regenerates a pseudo heatmap for supervision. Different from it, we argue that conducting a fusion on predicted heatmaps for the SSHPE task is harmful. We consider that this is because there are always differences in the estimation of keypoint positions for each I_{h_i} . It is an ill-posed problem to heuristically evaluate the consistency regularization contribution of each heatmap in pixel during ensemble. We explain and verify this in experiments.

Despite the simplicity, such a minor modification brings consistent gains over the original Single-Network under same SSL settings. With our discovered augmentation combinations T_{JOCO} and T_{JCCM} , the boosted Single-Network can surpass the original Dual-Network evidently. We have validated in ablation studies that the performance gain is non-trivial. We conjecture that regularizing multiple hard augmentations with a shared easy augmentation can be regarded as enforcing consistency among advanced augmentations as well, which inherits the concept of contrastive learning [6, 7, 15].

3.4. Our Overall Framework: MultiAugs

We leverage unlabeled images by applying multiple augmentations with integrating two key techniques introduced in Sec. 3.2 and Sec. 3.3. Firstly, assuming that we have obtained an optimal augmentation set $\widehat{\mathcal{T}}^n = \{\widehat{T}_{h_i}|_{i=1}^n\}$, where \widehat{T}_{h_i} may be an old single augmentation or a novel combined one. Then, we present how to construct our overall training framework (dubbed as MultiAugs) based on either the Single-Network or the Dual-Network.

MultiAugs (Single-Network). It is a consistency-based approach. We only need to maintain a single model during training. For each input batch with equal number of labeled images \mathbf{I}^l and unlabeled images \mathbf{I}^u , we calculate the supervised loss with the ground-truth heatmaps as in Eq. 1, and the multiple unsupervised losses as in Eq. 4, respectively. The final loss is obtained by adding the two loss functions $\mathcal{L} = \mathcal{L}_s + \lambda \mathcal{L}_u^*$ with $\lambda = 1$. Note that we only pass the gradient back through n hard augmentations $\widehat{\mathcal{T}}^n$ for generating teacher signals to avoid collapsing. Based on this boosted Single-Network, we complete all ablation experiments by changing the augmentation categories and quantities in $\widehat{\mathcal{T}}^n$ for controlling the unsupervised factor \mathcal{L}_u^* .

MultiAugs (Dual-Network). As shown in Fig. 5, this framework learns two identical yet independent networks with each similar to the Single-Network. For one input batch in every step, each of the two networks serves as both a teacher and a student. They both are fed by easy and hard augmentations of unlabeled images \mathbf{I}^u when they produce teacher signals and student signals, respectively. Assuming we have two networks f_A and f_B , and also the augmented easy images \mathbf{I}_e^u using T_e and n -path hard images

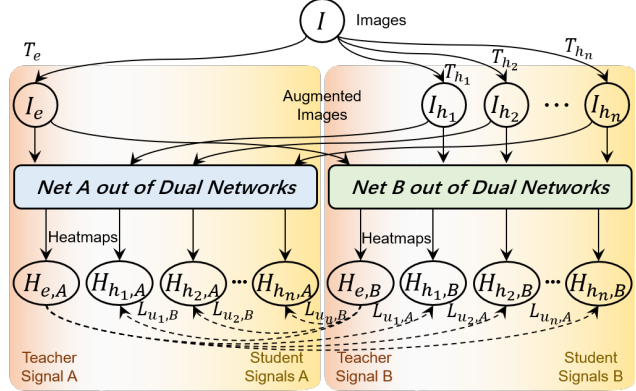


Figure 5. MultiAugs based on the Dual-Network, which utilizes multiple hard augmentations and generates multi-path consistency losses by facilitating cross training of two identical networks.

$\{\mathbf{I}_{h_1}^u, \mathbf{I}_{h_2}^u, \dots, \mathbf{I}_{h_n}^u\}$ using $\widehat{\mathcal{T}}^n$, we first predict the following four types of heatmaps:

$$\begin{aligned} \mathbf{H}_{e,A} &= T_{A30 \rightarrow A60}(f_A(\mathbf{I}_e^u)) \\ \mathbf{H}_{e,B} &= T_{A30 \rightarrow A60}(f_B(\mathbf{I}_e^u)) \\ \mathcal{H}_A &= \{\mathbf{H}_{h_i,A}|_{i=1}^n, \mathbf{H}_{h_i,A} = f_A(\mathbf{I}_{h_i}^u)\} \\ \mathcal{H}_B &= \{\mathbf{H}_{h_i,B}|_{i=1}^n, \mathbf{H}_{h_i,B} = f_B(\mathbf{I}_{h_i}^u)\} \end{aligned} \quad (5)$$

where $T_{A30 \rightarrow A60}$ is a pre-generated affine transformation. Based on above heatmaps, we calculate two unsupervised losses for training two networks as follows:

$$\begin{aligned} \mathcal{L}_{u,A}^* &= \mathbb{E}_{\mathbf{H}_{h_i,A} \in \mathcal{H}_A} \sum_{i=1}^n \|\mathbf{H}_{e,B} - \mathbf{H}_{h_i,A}\|^2 \\ \mathcal{L}_{u,B}^* &= \mathbb{E}_{\mathbf{H}_{h_i,B} \in \mathcal{H}_B} \sum_{i=1}^n \|\mathbf{H}_{e,A} - \mathbf{H}_{h_i,B}\|^2 \end{aligned} \quad (6)$$

where we swap positions of teacher signals $\mathbf{H}_{e,A}$ and $\mathbf{H}_{e,B}$ for realizing the cross training of networks f_B and f_A . Following [42], we report the average accuracy of the final two well-trained and performance-approached models. Besides, f_A and f_B can have different structures as in [17, 42], where the large one often helps to distill a better small model, but not vice versa. We do not intend to explore this consensus anymore in this paper.

4. Experiments

4.1. Datasets and Metrics

COCO. The dataset COCO [24] has 4 subsets: *train-set* (118K images), *val-set* (5K images), *test-dev* and *test-challenge*. It is a popular large-scale benchmark for human pose estimation, which contains over 150K annotated people. In addition, there are 123K wild unlabeled images (*wild-set*). We randomly selected 1K, 5K and 10K labeled data from *train-set*. In some experiments, unlabeled data came from the remaining images of *train-set*. In other experiments, we used the whole *train-set* as the labeled dataset

Table 1. AP of different methods on COCO *val-set* when different numbers of labels are used. Backbone is ResNet18.

Method	Net Num	1K	5K	10K	All
Supervised [39]	1	31.5	46.4	51.1	67.1
PseudoPose [42]	2	37.2	50.9	56.0	—
DataDistill [31]	2	37.6	51.6	56.6	—
PoseCons [42]	1	42.1	52.3	57.3	—
PoseDual [42]	2	44.6	55.6	59.6	—
SSPCM [17]	3	46.9	57.5	60.7	—
Ours (Single)	1	45.5	56.2	59.9	—
Ours (Dual)	2	49.7	58.8	61.8	—

and *wild-set* as the unlabeled dataset. The metric of mAP (Average AP over 10 OKS thresholds) is reported.

MPII and AI-Challenger. The dataset MPII [1] has 25K images and 40K person instances with 16 keypoints. The dataset AI-Challenger (AIC) [38] *train-set* has 210K images and 370K person instances with 14 keypoints. We use MPII as the labeled set, AIC as the unlabeled set. The metric of PCKh0.5 is reported.

4.2. Implementation Details

For a fair comparison with prior works, we use SimpleBaseline [39] to estimate heatmaps and ResNet [14] and HRNet [35] as backbones. The input image size is set to 256×192 . We adopt the PyTorch 1.30 and 4 A100 GPUs with each batch size as 32 for training. The initial learning rate is 1e-3. When training on COCO with 10K labeled data, it decreases to 1e-4 and 1e-5 at epochs 70 and 90, respectively, with a total of 100 epochs. When using 1K or 5K labeled data, total epochs are reduced to 30 or 70, respectively. When training on the complete COCO or MPII+AIC, it drops to 1e-4 and 1e-5 at epochs 220 and 260, respectively, with a total of 300 epochs. When testing, we do not flip horizontally.

For data augmentation settings, we keep the easy augmentation T_e as T_{A30} in all experiments. The chosen hard augmentations set is $\hat{\mathcal{T}}^4 = \{T_{JOCO}, T_{JCCM}, T_{JC}, T_{JO}\}$. We present details of finding two novel superior hard augmentations T_{JOCO} and T_{JCCM} , and selecting the optimal augmentation set $\hat{\mathcal{T}}^4$ in ablation studies.

4.3. Performance Comparison

We mainly compare our MultiAugs with SSHPE methods [17, 42] under five conditions:

(1) Firstly, we conduct experiments on the COCO *train-set* with 1K, 5K and 10K labeled data, and evaluate on the *val-set*. As shown in Tab. 1, our method brings substantial improvements under the same setting. For example, when using a Single-Network, our method exceeds both PoseCons and PoseDual significantly, and is close to the SSPCM based on three networks. When using a Dual-Network, our method exceeds previous SOTA results by **2.8** mAP, **1.3**

Table 2. Results on the COCO *val-set* when labeled images from the *train-set* and unlabeled images from the *wild-set*.

Method	Backbone	AP	AP. ₅	AR	AR. ₅
Supervised [39]	ResNet50	70.9	91.4	74.2	92.3
PoseDual [42]	ResNet50	73.9	92.5	77.0	93.5
SSPCM [17]	ResNet50	74.2	92.7	77.2	93.8
Ours (Single)	ResNet50	74.0	92.5	77.1	93.9
Ours (Dual)	ResNet50	74.6	93.5	77.6	94.0
Supervised [39]	ResNet101	72.5	92.5	75.6	93.1
PoseDual [42]	ResNet101	75.3	93.6	78.2	94.1
SSPCM [17]	ResNet101	75.5	93.8	78.4	94.2
Ours (Single)	ResNet101	75.4	93.4	78.4	94.1
Ours (Dual)	ResNet101	76.3	93.5	79.2	94.4
Supervised [39]	HRNet-w48	77.2	93.5	79.9	94.1
PoseDual [42]	HRNet-w48	79.2	94.6	81.7	95.1
SSPCM [17]	HRNet-w48	79.4	94.8	81.9	95.2
Ours (Single)	HRNet-w48	79.3	94.6	81.8	95.1
Ours (Dual)	HRNet-w48	79.5	94.6	82.1	95.2

Table 3. Comparison to the SOTA methods on the COCO *test-dev*. The COCO *train-set* is the labeled set and COCO *wild-set* is the unlabeled set. The person detection results are provided by SimpleBaseline and flipping strategy is used.

Method	Backbone	Input Size	AP	AR
SimpleBaseline [39]	ResNet50	256×192	70.2	75.8
HRNet [35]	HRNet-w48	384×288	75.5	80.5
MSPN [22]	ResNet50	384×288	76.1	81.6
DARK [50]	HRNet-w48	384×288	76.2	81.1
UDP [16]	HRNet-w48	384×288	76.5	81.6
TransPose-H-A6 [46]	HRNet-w48	256×192	75.0	—
TokenPose-L/D24 [23]	HRNet-w48	384×288	75.9	80.8
HRFormer [47]	HRFormer-B	384×288	76.2	81.2
ViTPose [43]	ViT-Base	256×192	77.3	—
DUAL (+HRNet) [42]	HRNet-w48	384×288	76.7	81.8
DUAL (+DARK) [42]	HRNet-w48	384×288	77.2	82.2
SSPCM (+DARK) [17]	HRNet-w48	384×288	77.5	82.4
Ours (Dual) (+HRNet)	HRNet-w48	384×288	76.8	81.8
Ours (Dual) (+DARK)	HRNet-w48	384×288	77.3	82.3

mAP, and **1.1** mAP under 1K, 5K and 10K settings, respectively. Note that our method can bring greater gains with less labeled data (*e.g.*, 1K images), which further explains its efficiency and superiority.

(2) Then, we conduct larger scale SSHPE experiments on the complete COCO dataset by using *train-set* as the labeled dataset and *wild-set* as the unlabeled dataset. The chosen optimal augmentations set is $\hat{\mathcal{T}}^2 = \{T_{JOCO}, T_{JCCM}\}$ for balancing training time and performance. As shown in Tab. 2, regardless of using any backbone, our method can always improve all supervised baseline results, and bring more gains than two compared SSHPE methods [42] and [17] with using dual networks. When using a single network, our method is still superior to PoseDual [42], and fairly close to SSPCM [17] based on triple networks.

Table 4. The results on the *val-set* of the MPII dataset. HRNet is trained only on the MPII *train-set*. The “*” means using extra labeled dataset AIC. The “+” means applying the model ensemble.

Method	Hea	Sho	Elb	Wri	Hip	Kne	Ank	Total
HRNet [35]	97.0	95.7	89.4	85.6	87.7	85.8	82.0	89.5
HRNet* [35]	97.4	96.7	92.1	88.4	90.8	88.6	85.0	91.7
PoseDual [42]	97.4	96.6	91.8	87.5	89.6	87.6	83.8	91.1
Ours (Dual)	97.3	96.8	91.7	87.5	90.3	88.6	84.6	91.4
Ours+ (Dual)	97.3	96.8	91.9	88.1	90.6	89.2	85.0	91.7

Table 5. Comparisons on the MPII *test-set* (PCKh0.5). Our method uses HRNetW32 as backbone and size is 256×256 . The MPII and AIC (w/o labels) dataset are used for training.

Method	Hea	Sho	Elb	Wri	Hip	Kne	Ank	Total
Newell <i>et al.</i> [26]	98.2	96.3	91.2	87.1	90.1	87.4	83.6	90.9
Xiao <i>et al.</i> [39]	98.5	96.6	91.9	87.6	91.1	88.1	84.1	91.5
Ke <i>et al.</i> [19]	98.5	96.8	92.7	88.4	90.6	89.4	86.3	92.1
Sun <i>et al.</i> [35]	98.6	96.9	92.8	89.0	91.5	89.0	85.7	92.3
Zhang <i>et al.</i> [52]	98.6	97.0	92.8	88.8	91.7	89.8	86.6	92.5
Xie <i>et al.</i> [42]	98.7	97.3	93.7	90.2	92.0	90.3	86.5	93.0
Huang <i>et al.</i> [17]	98.7	97.5	94.0	90.6	92.5	91.1	87.1	93.3
Ours (Dual)	98.8	97.6	94.1	90.3	92.4	91.1	87.2	93.4

(3) Besides, we also report our results using HRNet-w48 on the COCO *test-dev* in Tab. 3. Our method can slightly outperform the PoseDual but fall behind the best SSHPE. We attribute it to our fewer training epochs and less parameters which may lead to weaker generalization. Besides, we can observe that MultiAugs outperforms some burdensome transformer-based methods [23, 46, 47], which reveals the significance of rational utilization of unlabeled data.

(4) Finally, we allocate the MPII *train-set* as a labeled dataset and the whole AIC dataset as an unlabeled dataset. This is a more realistic setting where labeled and unlabeled images are from different datasets. Tab. 4 shows results on the *val-set* of MPII. Our approach outperforms both the supervised HRNet [35] and the semi-supervised PoseDual [42] by a large margin with using the same backbone. It is worth noting that our semi-supervised MultiAugs with applying the model ensemble can even approach the supervised HRNet with using extra labeled AIC dataset.

(5) Then, as shown in Tab. 5, our results on the MPII *test-set* surpass all those of previous fully supervised methods and two semi-supervised counterparts PoseDual and SSPCM. This further validates the effectiveness and superiority of our proposed method.

4.4. Ablation Studies

To further study our proposed MultiAugs, we conduct ablation experiments under the setting of COCO 1K with a total of 30 epochs. The learning rate drops 10 \times twice separately at epochs 20 and 25. All studied models take ResNet18 as the backbone, and follow the Single-Network framework.

Table 6. Best mAP results of different combinations.

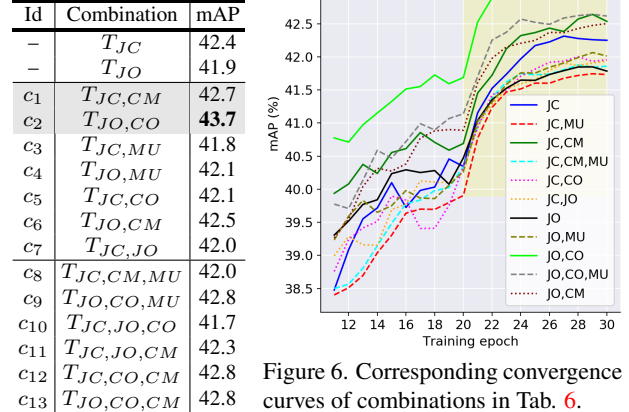


Figure 6. Corresponding convergence curves of combinations in Tab. 6.

Table 7. Best mAP results of different MultiAugs.

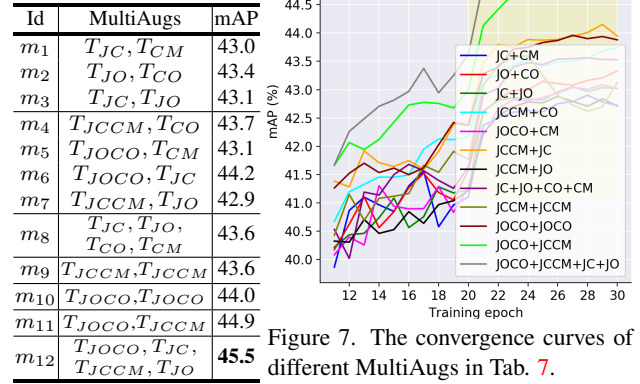


Figure 7. The convergence curves of different MultiAugs in Tab. 7.

4.4.1 Selection of Augmentations Combination.

In Sec. 3.2, we have explained the synergistic effects of different combinations of augmentations. Here, as shown in Tab. 6 and Fig. 6, we conducted various experiments about 13 selected combinations out of 26 choices. From these results, we can summarize three principles: (1) *The T_{MU} does cause adverse or inferior effects for each combination.* Please refer combinations with ids c_1 vs c_3 , c_2 vs c_4 , c_1 vs c_8 and c_2 vs c_9 . Thus, we do not add it for finding superior combinations. (2) *Synergistic effects between augmentations do exist.* Please refer combinations with ids c_1 vs c_5 , c_1 vs c_7 , c_2 vs c_6 and c_2 vs c_7 . Especially, the combination $T_{JC,JO}$ with two most advanced augmentations performs the worst among combinations $\{c_1, c_2, c_5, c_6, c_7\}$, which roundly reveals the harm of violating the principle of synergy. (3) *Do not overly combine too many augmentations.* Please refer combinations with ids c_1 vs c_{12} , c_2 vs c_{13} , c_1 vs c_{11} and c_2 vs c_{10} . Increasing the number of augmentations results in non-significant additional gain or even performance degradation. We attribute it to deviating from the rule of collaboration and severely damaging the

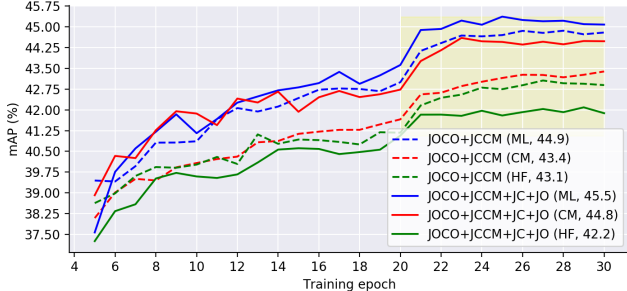


Figure 8. The convergence curves and best mAP results of two MultiAugs schemes with different training techniques.

structure of image. Based on above findings, we have sufficient reason not to enumerate the experimental results of rest combinations. And we recommend two new strongest combinations T_{JOCO} and T_{JCCM} .

4.4.2 Effectiveness of Multiple Augmentations.

In Sec. 3.3, we propose to optimize multi-path consistency losses of multiple differently augmented images simultaneously. Now, we experimentally verify the major advantage of this strategy as shown in Tab. 7 and Fig. 7. Here, we have two variables of MultiAugs: the number of paths and the category of augmentations. For acquisition of an optimal augmentations set, similarly, we continue with the rules summarized in the previous section, and elect 10 different MultiAugs schemes for illustrating. We can witness the effectiveness of MultiAugs from two aspects: (1) *It can inherit and even expand the synergistic effects between different augmentations.* (2) *It can alleviate the defects caused by excessive stacking of augmentations.* Please compare c_1 vs m_1 , c_2 vs m_2 and c_7 vs m_2 . MultiAugs provides comparable performance with the same augmentations. By comparing c_{10} vs m_6 , c_{11} vs m_7 , c_{12} vs m_4 and c_{13} vs m_5 , we can observe the sustained large improvement brought by MultiAugs. The scheme m_8 does not obtain a better result than m_{11} showing that new augmentations T_{JOCO} and T_{JCCM} have their essential properties. Schemes m_9 and m_{10} which utilize a single augmentation twice are also inferior to m_{11} showing the cooperativity of using multi-path distinct augmentations. Moreover, the optimal scheme m_{12} further unleashes capabilities of four advanced augmentations. In order to balance performance and time consumption, we do not add more augmentation paths.

4.4.3 Training Techniques of Multiple Heatmaps.

In this part, we present additional techniques commonly used for unsupervised consistency training. Especially, for predicted multiple heatmaps, we propose to optimize them by applying the multi-loss learning (ML) as in Eq. 4. Other two alternative techniques are *Confidence Masking* (CM) and *Heatmaps Fusion* (HF). For CM, the consistency loss

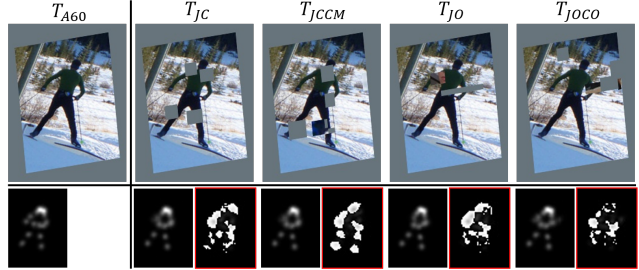


Figure 9. The predicted heatmaps of one easy augmentation (T_{A60}) and four hard augmentations in m_{10} . We also report the pixel-wise heatmap difference (with red borders) of each easy-hard pair to highlight subtle dissimilarities.

term in each minibatch is computed only on keypoint channels whose maximum activation value is greater than a threshold τ , which we set it to a high value 0.5. For HF, also termed as heatmaps ensemble, we sum the multi-path heatmaps and then average them to obtain a fused heatmap for loss computing. Then, we compare MultiAugs schemes (e.g., m_{11} and m_{12}) using either of these three techniques ML, CM and HF.

As shown in Fig. 8, our ML is strictly superior than the other two techniques under either MultiAugs scheme. For CM, we assume it may filter out some keypoint heatmaps with low confidence but high quality. This surely has a negative impact. For HF, although it has been widely used in other SSL tasks for models ensemble, it may not necessarily be applicable to our intermediate keypoint heatmaps. We deem this is because each predicted heatmap is distinctive and meaningful (see Fig. 9). It is tricky to replace them equivalently with a fused heatmap. In comparison, our multi-loss learning is a simple yet effective strategy.

5. Conclusions

In this paper, we consider to boost semi-supervised human pose estimation (SSHPE) from two perspectives: data augmentation and consistency training. Instead of inventing advanced augmentations in isolation, we attempt to synergistically combine existing augmentations, and handily generate novel superior combinations. The discovered combinations have intuitive interpretability and verified advantages in solving the SSHPE problem. For consistency training, we abandon the convention of growing the number of networks to increase unsupervised losses. We propose reusing a single network to generate corresponding multi-path unsupervised consistency losses for the same batch of unlabeled images. Combined with the optimal hard augmentations set, this plain and compact strategy is proven to be effective, and has leading performance on public benchmarks. Last but not least, we declare that the synergy effects of augmentations and multiple consistency losses are generic and generalizable for other SSL tasks such as classification and detection. We will explore them in the future.

References

[1] Mykhaylo Andriluka, Leonid Pishchulin, Peter Gehler, and Bernt Schiele. 2d human pose estimation: New benchmark and state of the art analysis. In *Proceedings of the IEEE Conference on Computer Vision and Pattern Recognition*, pages 3686–3693, 2014. [1](#), [3](#), [6](#)

[2] David Berthelot, Nicholas Carlini, Ian Goodfellow, Nicolas Papernot, Avital Oliver, and Colin A Raffel. Mixmatch: A holistic approach to semi-supervised learning. *Advances in Neural Information Processing Systems*, 32, 2019. [3](#)

[3] David Berthelot, Nicholas Carlini, Ekin D Cubuk, Alex Kurakin, Kihyuk Sohn, Han Zhang, and Colin Raffel. Remixmatch: Semi-supervised learning with distribution matching and augmentation anchoring. In *International Conference on Learning Representations*, 2020. [4](#)

[4] Zhe Cao, Tomas Simon, Shih-En Wei, and Yaser Sheikh. Realtime multi-person 2d pose estimation using part affinity fields. In *Proceedings of the IEEE Conference on Computer Vision and Pattern Recognition*, pages 7291–7299, 2017. [1](#), [2](#)

[5] Mathilde Caron, Ishan Misra, Julien Mairal, Priya Goyal, Piotr Bojanowski, and Armand Joulin. Unsupervised learning of visual features by contrasting cluster assignments. *Advances in Neural Information Processing Systems*, 33:9912–9924, 2020. [4](#)

[6] Ting Chen, Simon Kornblith, Mohammad Norouzi, and Geoffrey Hinton. A simple framework for contrastive learning of visual representations. In *International Conference on Machine Learning*, pages 1597–1607. PMLR, 2020. [5](#)

[7] Xinlei Chen and Kaiming He. Exploring simple siamese representation learning. In *Proceedings of the IEEE Conference on Computer Vision and Pattern Recognition*, pages 15750–15758, 2021. [5](#)

[8] Bowen Cheng, Bin Xiao, Jingdong Wang, Honghui Shi, Thomas S Huang, and Lei Zhang. Higherhrnet: Scale-aware representation learning for bottom-up human pose estimation. In *Proceedings of the IEEE Conference on Computer Vision and Pattern Recognition*, pages 5386–5395, 2020. [1](#), [2](#)

[9] Ekin D Cubuk, Barret Zoph, Dandelion Mane, Vijay Vasudevan, and Quoc V Le. Autoaugment: Learning augmentation policies from data. *arXiv preprint arXiv:1805.09501*, 2018. [3](#)

[10] Ekin D Cubuk, Barret Zoph, Jonathon Shlens, and Quoc V Le. Randaugment: Practical automated data augmentation with a reduced search space. In *Proceedings of the IEEE Conference on Computer Vision and Pattern Recognition Workshops*, pages 702–703, 2020. [2](#), [3](#)

[11] Terrance DeVries and Graham W Taylor. Improved regularization of convolutional neural networks with cutout. *arXiv preprint arXiv:1708.04552*, 2017. [2](#), [3](#), [4](#)

[12] Haodong Duan, Yue Zhao, Kai Chen, Dahua Lin, and Bo Dai. Revisiting skeleton-based action recognition. In *Proceedings of the IEEE Conference on Computer Vision and Pattern Recognition*, pages 2969–2978, 2022. [1](#)

[13] Hongyu Guo, Yongyi Mao, and Richong Zhang. Mixup as locally linear out-of-manifold regularization. In *Proceedings of the AAAI Conference on Artificial Intelligence*, pages 3714–3722, 2019. [2](#)

[14] Kaiming He, Xiangyu Zhang, Shaoqing Ren, and Jian Sun. Deep residual learning for image recognition. In *Proceedings of the IEEE Conference on Computer Vision and Pattern Recognition*, pages 770–778, 2016. [6](#)

[15] Kaiming He, Haoqi Fan, Yuxin Wu, Saining Xie, and Ross Girshick. Momentum contrast for unsupervised visual representation learning. In *Proceedings of the IEEE Conference on Computer Vision and Pattern Recognition*, pages 9729–9738, 2020. [5](#)

[16] Junjie Huang, Zheng Zhu, Feng Guo, and Guan Huang. The devil is in the details: Delving into unbiased data processing for human pose estimation. In *Proceedings of the IEEE Conference on Computer Vision and Pattern Recognition*, pages 5700–5709, 2020. [6](#)

[17] Linzhi Huang, Yulong Li, Hongbo Tian, Yue Yang, Xiangang Li, Weihong Deng, and Jieping Ye. Semi-supervised 2d human pose estimation driven by position inconsistency pseudo label correction module. In *Proceedings of the IEEE Conference on Computer Vision and Pattern Recognition*, pages 693–703, 2023. [1](#), [2](#), [3](#), [4](#), [5](#), [6](#), [7](#)

[18] Sam Johnson and Mark Everingham. Learning effective human pose estimation from inaccurate annotation. In *Proceedings of the IEEE Conference on Computer Vision and Pattern Recognition*, pages 1465–1472, 2011. [3](#)

[19] Lipeng Ke, Ming-Ching Chang, Honggang Qi, and Siwei Lyu. Multi-scale structure-aware network for human pose estimation. In *Proceedings of the European Conference on Computer Vision*, pages 713–728, 2018. [7](#)

[20] Zhanghan Ke, Daoye Wang, Qiong Yan, Jimmy Ren, and Rynson WH Lau. Dual student: Breaking the limits of the teacher in semi-supervised learning. In *Proceedings of the IEEE International Conference on Computer Vision*, pages 6728–6736, 2019. [3](#)

[21] Samuli Laine and Timo Aila. Temporal ensembling for semi-supervised learning. In *International Conference on Learning Representations*, 2016. [3](#)

[22] Wenbo Li, Zhicheng Wang, Binyi Yin, Qixiang Peng, Yuming Du, Tianzi Xiao, Gang Yu, Hongtao Lu, Yichen Wei, and Jian Sun. Rethinking on multi-stage networks for human pose estimation. *arXiv preprint arXiv:1901.00148*, 2019. [6](#)

[23] Yanjie Li, Shoukui Zhang, Zhicheng Wang, Sen Yang, Wankou Yang, Shu-Tao Xia, and Erjin Zhou. Tokenpose: Learning keypoint tokens for human pose estimation. In *Proceedings of the IEEE/CVF International Conference on Computer Vision*, pages 11313–11322, 2021. [6](#), [7](#)

[24] Tsung-Yi Lin, Michael Maire, Serge Belongie, James Hays, Pietro Perona, Deva Ramanan, Piotr Dollár, and C Lawrence Zitnick. Microsoft coco: Common objects in context. In *Proceedings of the European Conference on Computer Vision*, pages 740–755. Springer, 2014. [1](#), [3](#), [5](#)

[25] Olga Moskvyak, Frederic Maire, Feras Dayoub, and Mahsa Baktashmotagh. Semi-supervised keypoint localization. In *International Conference on Learning Representations*, 2021. [1](#), [3](#)

[26] Alejandro Newell, Kaiyu Yang, and Jia Deng. Stacked hourglass networks for human pose estimation. In *Proceedings*

of the European Conference on Computer Vision, pages 483–499. Springer, 2016. 7

[27] Avital Oliver, Augustus Odena, Colin A Raffel, Ekin Dogus Cubuk, and Ian Goodfellow. Realistic evaluation of deep semi-supervised learning algorithms. *Advances in Neural Information Processing Systems*, 31, 2018. 3

[28] Georgios Pavlakos, Luyang Zhu, Xiaowei Zhou, and Kostas Daniilidis. Learning to estimate 3d human pose and shape from a single color image. In *Proceedings of the IEEE Conference on Computer Vision and Pattern Recognition*, pages 459–468, 2018. 1

[29] Georgios Pavlakos, Vasileios Choutas, Nima Ghorbani, Timo Bolkart, Ahmed AA Osman, Dimitrios Tzionas, and Michael J Black. Expressive body capture: 3d hands, face, and body from a single image. In *Proceedings of the IEEE Conference on Computer Vision and Pattern Recognition*, pages 10975–10985, 2019. 1

[30] Siyuan Qiao, Wei Shen, Zhishuai Zhang, Bo Wang, and Alan Yuille. Deep co-training for semi-supervised image recognition. In *Proceedings of the European Conference on Computer Vision*, pages 135–152, 2018. 3

[31] Ilija Radosavovic, Piotr Dollár, Ross Girshick, Georgia Gkioxari, and Kaiming He. Data distillation: Towards omni-supervised learning. In *Proceedings of the IEEE Conference on Computer Vision and Pattern Recognition*, pages 4119–4128, 2018. 3, 4, 6

[32] M Saquib Sarfraz, Arne Schumann, Andreas Eberle, and Rainer Stiefelhagen. A pose-sensitive embedding for person re-identification with expanded cross neighborhood re-ranking. In *Proceedings of the IEEE Conference on Computer Vision and Pattern Recognition*, pages 420–429, 2018. 1

[33] Kihyuk Sohn, David Berthelot, Nicholas Carlini, Zizhao Zhang, Han Zhang, Colin A Raffel, Ekin Dogus Cubuk, Alexey Kurakin, and Chun-Liang Li. Fixmatch: Simplifying semi-supervised learning with consistency and confidence. *Advances in Neural Information Processing Systems*, 33:596–608, 2020. 3

[34] Matthias Springstein, Stefanie Schneider, Christian Althaus, and Ralph Ewerth. Semi-supervised human pose estimation in art-historical images. In *Proceedings of the 30th ACM International Conference on Multimedia*, pages 1107–1116, 2022. 3

[35] Ke Sun, Bin Xiao, Dong Liu, and Jingdong Wang. Deep high-resolution representation learning for human pose estimation. In *Proceedings of the IEEE Conference on Computer Vision and Pattern Recognition*, pages 5693–5703, 2019. 1, 2, 6, 7

[36] Antti Tarvainen and Harri Valpola. Mean teachers are better role models: Weight-averaged consistency targets improve semi-supervised deep learning results. *Advances in Neural Information Processing Systems*, 30, 2017. 3

[37] Can Wang, Sheng Jin, Yingda Guan, Wentao Liu, Chen Qian, Ping Luo, and Wanli Ouyang. Pseudo-labeled auto-curriculum learning for semi-supervised keypoint localization. In *International Conference on Learning Representations*, 2022. 1, 3

[38] Jiahong Wu, He Zheng, Bo Zhao, Yixin Li, Baoming Yan, Rui Liang, Wenjia Wang, Shipei Zhou, Guosen Lin, Yanwei Fu, et al. Large-scale datasets for going deeper in image understanding. In *2019 IEEE International Conference on Multimedia and Expo (ICME)*, pages 1480–1485. IEEE, 2019. 1, 6

[39] Bin Xiao, Haiping Wu, and Yichen Wei. Simple baselines for human pose estimation and tracking. In *Proceedings of the European Conference on Computer Vision*, pages 466–481, 2018. 1, 2, 6, 7

[40] Qizhe Xie, Zihang Dai, Eduard Hovy, Thang Luong, and Quoc Le. Unsupervised data augmentation for consistency training. *Advances in Neural Information Processing Systems*, 33:6256–6268, 2020. 3

[41] Qizhe Xie, Minh-Thang Luong, Eduard Hovy, and Quoc V Le. Self-training with noisy student improves imagenet classification. In *Proceedings of the IEEE Conference on Computer Vision and Pattern Recognition*, pages 10687–10698, 2020. 3

[42] Rongchang Xie, Chunyu Wang, Wenjun Zeng, and Yizhou Wang. An empirical study of the collapsing problem in semi-supervised 2d human pose estimation. In *Proceedings of the IEEE International Conference on Computer Vision*, pages 11240–11249, 2021. 1, 2, 3, 4, 5, 6, 7

[43] Yufei Xu, Jing Zhang, Qiming Zhang, and Dacheng Tao. Vitpose: Simple vision transformer baselines for human pose estimation. *Advances in Neural Information Processing Systems*, 35:38571–38584, 2022. 1, 2, 6

[44] Sijie Yan, Yuanjun Xiong, and Dahua Lin. Spatial temporal graph convolutional networks for skeleton-based action recognition. In *Proceedings of the AAAI Conference on Artificial Intelligence*, 2018. 1

[45] Jie Yang, Ailing Zeng, Shilong Liu, Feng Li, Ruimao Zhang, and Lei Zhang. Explicit box detection unifies end-to-end multi-person pose estimation. *International Conference on Learning Representations*, 2023. 1, 2

[46] Sen Yang, Zhibin Quan, Mu Nie, and Wankou Yang. Transpose: Keypoint localization via transformer. In *Proceedings of the IEEE/CVF International Conference on Computer Vision*, pages 11802–11812, 2021. 6, 7

[47] Yuhui Yuan, Rao Fu, Lang Huang, Weihong Lin, Chao Zhang, Xilin Chen, and Jingdong Wang. Hrformer: High-resolution transformer for dense prediction. *Advances in Neural Information Processing Systems*, 34:7281–7293, 2021. 6, 7

[48] Sangdoo Yun, Dongyoon Han, Seong Joon Oh, Sanghyuk Chun, Junsuk Choe, and Youngjoon Yoo. Cutmix: Regularization strategy to train strong classifiers with localizable features. In *Proceedings of the IEEE International Conference on Computer Vision*, pages 6023–6032, 2019. 2, 3, 4

[49] Bowen Zhang, Yidong Wang, Wenxin Hou, Hao Wu, Jindong Wang, Manabu Okumura, and Takahiro Shinozaki. Flexmatch: Boosting semi-supervised learning with curriculum pseudo labeling. *Advances in Neural Information Processing Systems*, 34:18408–18419, 2021. 3

[50] Feng Zhang, Xiatian Zhu, Hanbin Dai, Mao Ye, and Ce Zhu. Distribution-aware coordinate representation for human pose estimation. In *Proceedings of the IEEE Conference*

on Computer Vision and Pattern Recognition, pages 7093–7102, 2020. 6

- [51] Hongyi Zhang, Moustapha Cisse, Yann N Dauphin, and David Lopez-Paz. mixup: Beyond empirical risk minimization. In *International Conference on Learning Representations*, 2018. 2, 4
- [52] Hong Zhang, Hao Ouyang, Shu Liu, Xiaojuan Qi, Xiaoyong Shen, Ruigang Yang, and Jiaya Jia. Human pose estimation with spatial contextual information. *arXiv preprint arXiv:1901.01760*, 2019. 7
- [53] Haiyu Zhao, Maoqing Tian, Shuyang Sun, Jing Shao, Junjie Yan, Shuai Yi, Xiaogang Wang, and Xiaoou Tang. Spindle net: Person re-identification with human body region guided feature decomposition and fusion. In *Proceedings of the IEEE Conference on Computer Vision and Pattern Recognition*, pages 1077–1085, 2017. 1